KSME

Springer

Journal of Mechanical Science and Technology 34 (6) 2020

Original Article
DOI 10.1007/s12206-020-0533-5

Keywords:
· Two-link robot manipulator
· Counterweight
· Point-to-point motion
· Optimal control
· Zero-power balancing

Correspondence to:
Amin Nikoobin
anikoobin@semnan.ac.ir

Citation:
Vezvari, M. R., Nikoobin, A., Ghoddosian, A. (2020). Zero-power balancing a two-link robot manipulator for a predefined point-to-point task. Journal of Mechanical Science and Technology 34 (6) (2020) 2585~2595.
http://doi.org/10.1007/s12206-020-0533-5

Received June 26th, 2019
Revised December 18th, 2019
Accepted March 21st, 2020

† Recommended by Editor
Ja Choon Koo

Zero-power balancing a two-link robot manipulator for a predefined point-to-point task

Mojtaba Riyahi Vezvari[1], Amin Nikoobin[1] and Ali Ghoddosian[2]

[1]Robotics and Control Lab, Faculty of Mechanical Engineering, Semnan University, Semnan, Iran, [2]Faculty of Mechanical Engineering, Semnan University, Semnan, Iran

Abstract In this paper, a new balancing approach called "zero-power balancing" (ZPB) method is presented for a two-link robot manipulator (TLRM) whose end-effector must move on a vertical plane between two given points repeatedly. To this purpose, a simple balancing mechanism which has two adjustable degrees of freedom is presented by which the required power will be zero and the proposed method can be applied for any specific boundary conditions. In order to solve the problem, balancing problem is formulated as an optimal control problem on which the required optimality conditions were derived using the Pontryagin's minimum principle, leading to a two-point boundary value problem (TPBVP). By solving the obtained TPBVP, states, controls and the constant parameters of the counterweights were simultaneously determined. By considering the performance index as minimum effort, it was interestingly observed that the values of torque at joints vanished perfectly and identical counterweight's specifications were obtained in forward and return motions, so that the manipulator could swing between the two given points freely. Capability of the proposed method to implement the swinging motion between the two desired points was illustrated via simulation. Due to friction, air resistance, and parametric uncertainties, it was practically difficult to implement the motion repeatedly and at no power consumption as an open-loop policy, but rather two small actuators are required to control the manipulator along the optimal trajectory. Finally, an experimental set-up was developed to validate the simulation results and illustrated the efficiency of the ZPB method.

1. Introduction

As an efficient way to increase the performance of a robot, balancing refers to a well-known challenge in the field of mechanical engineering [1]. A review on related literature shows that a robotic system can be balanced via two classes of approach: Task-independent and task-dependent approaches. The task-independent balancing methods (TIBMs) are performed without considering the traveling trajectory. Three types of TIBMs have been developed so far: Static balancing, adaptive balancing and dynamic balancing. In static balancing, it is assumed that the weight of the links exerts no force onto actuators for any configuration of the manipulator, i.e., constant potential energy for all possible configurations [2]. Applying some modifications to unbalanced mechanisms, adaptive balancing attempts to obtain static balancing and complete decoupling of dynamic equations [3]. In dynamic balancing, the reaction forces and reaction moments vanish for any motion. Indeed, the shaking force and shaking moment of the manipulator are compensated for by the dynamic balancing [4]. For most part, this method is used for parallel manipulators. Moradi et al. proposed a systematic adaptive approach for open-chain planar robots with their links connected by revolute joints [5]. Cho and Kang proposed a design method for a gravity compensator using unit spring balancers for a multi-degree of freedom (DOF) multi-link manipulator [6]. Chaudhary et al. presented an optimization technique to dynamically balance the planar mechanisms in which the shaking forces and shaking moments

were minimized using the genetic algorithm [7]. Veer and Sujatha presented a new method where approximate gravity balancing was implemented to reduce actuator loads. This new method allowed springs to be attached to the preceding parent link [8]. Chen et al. presented a methodology for combining counterweight and actuator torque. This method could lead to a considerable reduction in the required actuator torque, thereby favoring the implementation of the dynamic balancing [9]. Boisclair et al. used the concentric motion of Halbach cylinders to produce a joint torque that could compensate the torque produced by a gravitational load precisely [10]. Kumani et al. presented the octahedron seven point masses model and "teaching-learning-based optimization" technique to minimize constraint forces and moments at joints of an industrial manipulator [11]. Zhang et al. proposed an analytically tractable solution to gravity balancing a planar four-bar linkage. They provided an optimal generation of the balancing developed by a non-zero length spring [12]. Yun et al. introduced a new balance method based on the identification of energy transfer coefficient of spindle rotor system [13]. Martini et al. presented an approach to statically balance of open and closed kinematic chains. The proposed algorithm determines the balance arrangement by installing combinations of counterweights and springs [14].

Unlike the TIBMs, in the task-dependent balancing methods (TDBMs), the balancing is performed for a given task. Ravichandran et al. presented a method for simultaneously optimizing the values of counterweights and gains of a nonlinear PD controller for a two-link robot manipulator (TLRM) performing a given task [15]. Nikoobin et al. presented an optimal balancing method where states, controls, and all unknown parameters associated with the counterweights or springs were calculated simultaneously to minimize the performance index for a point-to-point motion [16]. They developed the proposed method for counterweight-balanced robot manipulators [17], spring-balanced robot manipulators [18], planar cable robot [19] and spatial cable robot [20]. Moradi et al. utilized a closed-loop method for addressing optimal control problem to find the optimal controller/parameters of an open-chain robot manipulator in point-to-point motion [21].

Once the trajectory planning problem is further introduced into TDBM, special methods are required to solve the problem. For this purpose, two categories of methods have been distinguished: Direct and indirect methods [22]. Direct methods are based on discretization of dynamic variables (states, controls) and result in a parameter optimization problem. Then, evolutionary, non-linear optimization or classical stochastic techniques are applied to obtain optimal values of the parameters. However, these techniques lead to an approximate solution of the optimization problem and often suffer from numerical explosion when encountering problems of large dimensions. The indirect methods are based on Pontryagin's minimum principle (PMP), in which the optimality conditions are expressed as a set of differential equations. By solving the obtained two-point boundary value problem (TPBVP), one can obtain the exact solution of the optimal control problem. This method has been widely used as a powerful and efficient tool for analyzing nonlinear systems and trajectory planning for different types of system [23, 24]. Ghasemi et al. used the indirect solution of an open-loop optimal control problem so that the problem is translated to a non-linear TPBVP. By using an iterative method, the time-optimal point-to-point control is computed for a robot manipulator [25]. Gong et al. performed a study on the optimal control to find optimal pose at target for a planar three-DOF manipulator. Accordingly, they reached an optimal trajectory for which the torque was minimized while dynamics was taken into consideration [26].

By reviewing the previous work, it is found that most of the work dealing with the balancing of robotic systems are listed in the TIBMs [2-14]. In the previous studies used TDBMs, the torque was minimized rather than being actually vanished. Due to the proposed balancing mechanism which has two adjustable degrees of freedom, the required power will be zero and the proposed method can be applied for any specific boundary conditions. The previous studies on the balancing tend to solely minimize the torques rather than having it vanished, while the ZPB method vanishes the torque at the joints. In order to solve the problem, optimal balancing problem is formulated as an optimal control problem. Since solving the optimal control problem by indirect method results in exact solution, PMP is applied to derive the required optimality conditions. Finally, the obtained TPBVP is solved to determine the states, controls and the constant parameters of the counterweights.

This paper is organized into four sections. In Sec. 2, formulation of the ZPB approach is presented and the dynamic governing equations for a TLRM are derived by considering the counterweights. In order to verify the proposed methodology, simulation and experimental results are presented in Sec. 3. Finally, Sec. 4 draws conclusions out of this study.

2. Formulation of zero-power balancing

In this section, a new balancing approach called "zero-power balancing" (ZPB) method is introduced for the TLRM. This method improves the dynamic performance of the robot. In this method, counterweights, the robot trajectory, and the torque at each joint must be evaluated simultaneously in such a way to achieve zero performance index for a predefined point-to-point task. The point-to-point motion is a repetitive motion between two given positions. This motion contains forward and return motions. For the forward motion, the robot moves from the start position to end position. Then, in the return motion, the robot moves from the end position to start position. The point-to-point motion uses in many applications, one which is pick-and-place operation. For implementation of the ZPB method, the optimal control method can be used to obtain necessary conditions for optimality [27].

2.1 Dynamic modeling of TLRM with counterweights

In this paper, a robot with the counterweights shown in Fig. 1

Table 1. Parameters of the robot.

Global coordinate	*XOY*
Mass and length of link *i*	m_i , l_i ; i = 1,2
Position of the center of mass of link *i*	r_i ; i = 1,2
Joint angle of link *i*	θ_i ; i = 1,2
Mass and length of counterweight *i*	m_{ci} , l_{ci} ; i = 1,2
Installation angle of counterweight *i* relative to link *i*	β_i ; i = 1,2
Gravitational acceleration	*g*

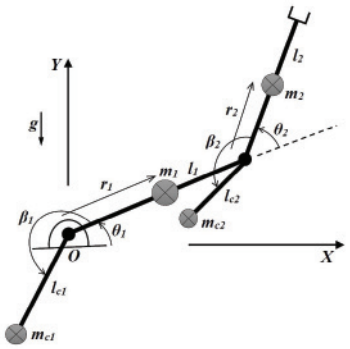

Fig. 1. A schematic view of the considered TLRM with the counterweights.

was considered. As shown on the figure, two counterweights were attached to the links 1 and 2. Herein m_{ci}, l_{ci} and β_i (i = 1, 2) are mass, length, and installation angle of the counterweight *i* with reference to the link *i*, respectively. The parameters of the TLRM shown in Fig. 1 are introduced in Table 1.

The Lagrange's method was used to obtain the dynamic equation. This method is written in terms of the Lagrangian function *L*, the generalized coordinate *q*, and the generalized force or torque *Q*, as follows:

$$\frac{d}{dt}\left(\frac{\partial L}{\partial \dot{q}}\right)-\frac{\partial L}{\partial q}=Q. \tag{1}$$

By definition, function *L* evaluates the difference between kinetic and potential energies of a system; i.e., $L = K-U$, where *K* is the kinetic energy and *U* is the potential energy of the system, both written in terms of generalized coordinates *q*. For the TLRM, generalized coordinate and generalized torque in Eq. (1) are defined as follows:

$$q=\theta=[\theta_1\ \ \theta_2]^T\ ,\ Q=\tau=[\tau_1\ \ \tau_2]^T \tag{2}$$

where *τ* is the applied torque at joint. For the TLRM, the kinetic and potential energies can be obtained as follows:

$$K=\frac{1}{2}mv^2+\frac{1}{2}I\omega^2\ ,\ U=mgh \tag{3}$$

where *m*, *I*, *v*, and *ω* are mass, moment of inertia, linear velocity, and angular velocity of the considered part of robot, respectively. Moreover, *h* is the height of the center of mass. For calculating the kinetic and potential energies of the robot, the following steps were undertaken.

At first, positions of the center of masses were determined in the global coordinate system.

$$\begin{aligned}
&x_1=r_1\cos\theta_1\ ,y_1=r_1\sin\theta_1\\
&x_2=l_1\cos\theta_1+r_2\cos(\theta_1+\theta_2)\ ,y_2=l_1\sin\theta_1+r_2\sin(\theta_1+\theta_2)\\
&x_{c1}=l_{c1}\cos(\theta_1+\beta_1)\ ,y_{c1}=l_{c1}\sin(\theta_1+\beta_1)\\
&x_{c2}=l_1\cos\theta_1+l_{c2}\cos(\theta_1+\theta_2+\beta_2)\ ,\\
&y_{c2}=l_1\sin\theta_1+l_{c2}\sin(\theta_1+\theta_2+\beta_2)
\end{aligned} \tag{4}$$

where x_i and y_i (i = 1, 2) are the coordinates of the center of mass of the link *i* in directions *X* and *Y*, respectively, and x_{ci} and y_{ci} (i = 1, 2) are the coordinates of the mass of the counterweight *i* in directions *X* and *Y*, respectively. Then, by taking derivative of the above equation with respect to time, velocities of the centers of mass were obtained as follows:

$$\begin{aligned}
&\dot{x}_1=-r_1\dot{\theta}_1\sin\theta_1\ ,\ \dot{y}_1=r_1\dot{\theta}_1\cos\theta_1\\
&\dot{x}_2=-l_1\dot{\theta}_1\sin\theta_1-r_2(\dot{\theta}_1+\dot{\theta}_2)\sin(\theta_1+\theta_2)\ ,\\
&\dot{y}_2=l_1\dot{\theta}_1\cos\theta_1+r_2(\dot{\theta}_1+\dot{\theta}_2)\cos(\theta_1+\theta_2)\\
&\dot{x}_{c1}=-l_{c1}\dot{\theta}_1\sin(\theta_1+\beta_1)\ ,\ \dot{y}_{c1}=l_{c1}\dot{\theta}_1\cos(\theta_1+\beta_1)\\
&\dot{x}_{c2}=-l_1\dot{\theta}_1\sin\theta_1-l_{c2}(\dot{\theta}_1+\dot{\theta}_2)\sin(\theta_1+\theta_2+\beta_2)\ ,\\
&\dot{y}_{c2}=l_1\dot{\theta}_1\cos\theta_1+l_{c2}(\dot{\theta}_1+\dot{\theta}_2)\cos(\theta_1+\theta_2+\beta_2).
\end{aligned} \tag{5}$$

Finally, the kinetic and potential energies (*K, U*) of the robot were evaluated as follows:

$$\begin{aligned}
&k=\frac{1}{2}\sum_{i=1}^{2}(m_iv_i^2+I_i\omega_i^2)\ ,\ k_c=\frac{1}{2}\sum_{i=1}^{2}m_{ci}v_{ci}^2\ ;\\
&v_i^2=\dot{x}_i^2+\dot{y}_i^2\ ,\ v_{ci}^2=\dot{x}_{ci}^2+\dot{y}_{ci}^2\ ;\ i=1,2\ ,\ \omega_1=\dot{\theta}_1\ ,\ \omega_2=\dot{\theta}_1+\dot{\theta}_2\\
&u=m_1gr_1\sin\theta_1+m_2g(l_1\sin\theta_1+r_2\sin(\theta_1+\theta_2))\ ,\\
&u_c=m_{c1}gl_{c1}\sin(\theta_1+\beta_1)+m_{c2}g(l_1\sin\theta_1+l_{c2}\sin(\theta_1+\theta_2+\beta_2))\\
&K=k+k_c\ ,\ U=u+u_c
\end{aligned} \tag{6}$$

where *k* and *u* are the kinetic and potential energies of the two links of the robot, respectively, and k_c and u_c are the kinetic and potential energies of the two counterweights of the robot, respectively. By substituting Eq. (6) into Eq. (1), the final dynamic equation of the robot was obtained as follows:

$$M\ddot{\theta}+N+G=\tau\ ;\ \ddot{\theta}=[\ddot{\theta}_1\ \ \ddot{\theta}_2]^T\ ,\tau=[\tau_1\ \ \tau_2]^T, \tag{7}$$

where *M*, *N* and *G* are the matrix of inertia, the Coriolis and centrifugal terms, and gravity terms, respectively.

2.2 The ZPB methodology

In this section, implementation of the ZPB method for the TLRM is presented. The ZPB uses the optimal control problem

by defining the state vector as follows:

$$x=\left[q^T\ \ \dot{q}^T\right]^T \xrightarrow{q=[\theta_1\ \theta_2]^T,\ \dot{q}=[\dot{\theta}_1\ \dot{\theta}_2]^T} x=\left[\theta_1\ \ \theta_2\ \ \dot{\theta}_1\ \ \dot{\theta}_2\right]^T. \tag{8}$$

By rewriting the above equation, the final form of the state vector x is obtained as follows:

$$x=\left[\theta_1\ \ \theta_2\ \ \dot{\theta}_1\ \ \dot{\theta}_2\right]^T \xrightarrow{x_1=\theta_1,\ x_2=\theta_2,\ x_3=\dot{\theta}_1,\ x_4=\dot{\theta}_2} x=\left[x_1\ \ x_2\ \ x_3\ \ x_4\right]^T. \tag{9}$$

The dynamic Eq. (7) can be rewritten in state-space form as:

$$f=\dot{x} \xrightarrow{\dot{x}=\left[\dot{\theta}_1\ \dot{\theta}_2\ \ddot{\theta}_1\ \ddot{\theta}_2\right]^T}$$
$$f=\begin{bmatrix} x_3 \\ x_4 \\ M_{2\times2}^{-1}(x_1,x_2,b)\left[\tau-N(x,b)-G(x_1,x_2,b)\right]_{2\times1}\end{bmatrix} \tag{10}$$

where f is continuous on x and τ, and continuously differentiable with respect to x, and b is the vector of design parameters. The vector b contains the unknown constant parameters of the model. Then Hamiltonian function is written as follows:

$$H=F+\psi^T f. \tag{11}$$

In Eq. (11), ψ is the co-state vector and F is the integrand of the performance index. For the TLRM, the control-effort vector and the time interval are $u=[\tau_1\ \tau_2]^T$ and $t=[0\ t_f]$, respectively. Defining the performance index as the following minimum-effort:

$$J=\int_0^{t_f} F\,dt=\int_0^{t_f}(\tau_1^2+\tau_2^2)\,dt, \tag{12}$$

and the co-state vector as follows:

$$\psi=\left[\psi_1^T\ \ \psi_2^T\right]^T \xrightarrow{\psi_1=[x_5\ x_6]^T,\ \psi_2=[x_7\ x_8]^T} \psi=\left[x_5\ \ x_6\ \ x_7\ \ x_8\right]^T, \tag{13}$$

the Hamiltonian function becomes

$$H=(\tau_1^2+\tau_2^2)+x_5x_3+x_6x_4+\left[x_7\ \ x_8\right]\times \left[M_{2\times2}^{-1}(x_1,x_2,b)\left[\tau-N(x,b)-G(x_1,x_2,b)\right]_{2\times1}\right]_{2\times1}. \tag{14}$$

The value of J is placed between zero to positive infinity. The lower the performance index J, the better the performance of the robot. Using the PMP, the optimality conditions are defined as follows:

$$\dot{x}=H_\psi=\left[\frac{\partial H}{\partial\psi_1}\ \ \frac{\partial H}{\partial\psi_2}\right]^T\rightarrow \dot{x}=f, \tag{15}$$

$$\dot{\psi}=-H_x\rightarrow\dot{\psi}=[\dot{x}_5\ \dot{x}_6\ \dot{x}_7\ \dot{x}_8]^T= -\left[\frac{\partial H}{\partial x_1}\ \frac{\partial H}{\partial x_2}\ \frac{\partial H}{\partial x_3}\ \frac{\partial H}{\partial x_4}\right]^T, \tag{16}$$

$$H_u=0\rightarrow\frac{\partial H}{\partial\tau_1}=0,\ \frac{\partial H}{\partial\tau_2}=0, \tag{17}$$

subject to the following boundary condition:

$$\begin{aligned} &x(0)=x_0,\ x(t_f)=x_f\rightarrow\\ &x(0)=\left[x_1(0)\ \ x_2(0)\ \ x_3(0)\ \ x_4(0)\right]^T=\left[\theta_{10}\ \ \theta_{20}\ \ 0\ \ 0\right]^T,\\ &x(t_f)=\left[x_1(t_f)\ \ x_2(t_f)\ \ x_3(t_f)\ \ x_4(t_f)\right]^T=\left[\theta_{1f}\ \ \theta_{2f}\ \ 0\ \ 0\right]^T. \end{aligned} \tag{18}$$

In the above equation, θ_0 is the initial angle at $t = 0$ and θ_f is the final angle at $t = t_f$. For point-to-point motion, the initial and final angular velocities are assumed to be zero ($\dot{\theta}_0=\dot{\theta}_f=0$).

The optimal control can be used to obtain the optimal values of the vector b. This vector contains some system parameters. This is performed by defining a new state vector called μ [16]. Therefore, optimum trajectory planning is implemented based on unknown parameters of the robot. In the ZPB, the parameters m_{c1}, m_{c2}, β_1 and β_2 are taken as unknown variables of the counterweights.

Thus, by considering the vector of parameters as follows:

$$b=\left[m_{c1}\ \ m_{c2}\ \ \beta_1\ \ \beta_2\right], \tag{19}$$

the new state vector μ is defined as below:

$$\mu=\left[x_9\ \ x_{10}\ \ x_{11}\ \ x_{12}\right]^T. \tag{20}$$

The optimality and boundary conditions associated with the vector μ are obtained as follows:

$$\begin{aligned} &\dot{\mu}=-H_b\rightarrow\dot{x}_9=-\frac{\partial H}{\partial m_{c1}},\ \dot{x}_{10}=-\frac{\partial H}{\partial m_{c2}},\\ &\dot{x}_{11}=-\frac{\partial H}{\partial\beta_1},\ \dot{x}_{12}=-\frac{\partial H}{\partial\beta_2} \end{aligned} \tag{21}$$

$$\begin{aligned} &\mu(t_0)=\mu(t_f)=0\rightarrow x_9(0)=x_{10}(0)=x_{11}(0)=x_{12}(0)=\\ &x_9(t_f)=x_{10}(t_f)=x_{11}(t_f)=x_{12}(t_f)=0. \end{aligned} \tag{22}$$

Finally, by substituting τ_1 and τ_2 from Eq. (17) into Eqs. (15), (16) and (21), a total of 12 nonlinear ordinary differential equations are derived. Constrained to the 16 boundary conditions given in Eqs. (18) and (22), these equations construct a two-point boundary value problem (TPBVP). This TPBVP is solved using the bvp4c command in MATLAB software to determine the state vector x, co-state vector ψ, new state vector μ and parameters vector b.

Also, to obtain the static balancing, the gravity terms $G = [G_1\ G_2]^T$ must be achieved to zero. So, the counterweights parameters are obtained as follows:

Table 2. Parameters of the examined TLRM.

Parameter	Value
Mass (kg)	$m_1 = 0.171$, $m_2 = 0.208$, $m_{c1} = 0.1$, $m_{c2} = 0.05$
Length (m)	$l_1 = 0.091$, $l_2 = 0.067$
Position of the center of mass (m)	$r_1 = 0.042$, $r_2 = 0.0384$, $l_{c1} = 0.07$, $l_{c2} = 0.05$
Moment of inertia (kg.m^2)	$I_1 = 0.32e\text{-}3$, $I_2 = 0.24e\text{-}3$
Installation angle of counterweight (rad)	$\beta_1 = \pi$, $\beta_2 = \pi$
Gravitational acceleration (m/s^2)	$g = 9.81$

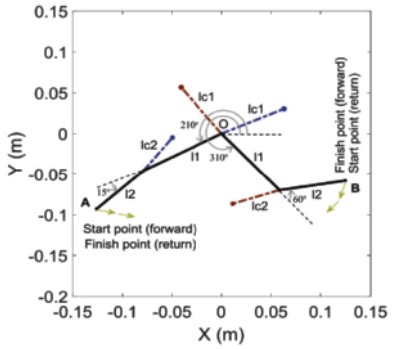

Fig. 2. The start and end positions of the robot.

$$\beta_1 = \pi,\ \beta_2 = \pi,\ m_{c2} = \frac{m_2 r_2}{l_{c2}},\ m_{c1} = \frac{m_1 r_1 + m_2 l_1 + m_{c2} l_1}{l_{c1}}. \tag{23}$$

3. Simulation and experimental results

In this section, results of simulating the TLRM shown in Fig. 1 are presented. Two cases were considered for this purpose: Unbalanced and zero-power balanced. In the unbalanced case, counterweights were zero (m_{c1} = m_{c2} = 0). The experimental set-up presented in Sec. 3.2 is based on the robot parameter values given in Table 2. Simulations and experiments were performed for different point-to-point motions. For both unbalanced and ZPB cases, the theoretical results were compared to experimental data.

3.1 Theoretical simulation

Consider a repetitive point-to-point motion with the following boundary conditions for the forward motion,

$$\begin{aligned} &x_1(0) = 210\ ^\circ,\ x_1(t_f) = 310\ ^\circ,\ x_2(0) = 15\ ^\circ,\ x_2(t_f) = 60\ ^\circ \\ &x_3(0) = x_3(t_f) = x_4(0) = x_4(t_f) = 0,\ t_f = 0.75s, \end{aligned} \tag{24}$$

and the following boundary conditions for the return motion:

$$\begin{aligned} &x_1(0) = 310\ ^\circ,\ x_1(t_f) = 210\ ^\circ,\ x_2(0) = 60\ ^\circ,\ x_2(t_f) = 15\ ^\circ \\ &x_3(0) = x_3(t_f) = x_4(0) = x_4(t_f) = 0,\ t_f = 0.75s. \end{aligned} \tag{25}$$

By solving the TPBVP obtained in Sec. 2.2, the joint angular positions and velocities and the values of m_{c1}, m_{c2}, β_1 and β_2 of the counterweights could be obtained. The start and finish positions of the TLRM with the counterweights are shown in Fig. 2. For the forward motion, the end-effector of the robot moves from *A* to *B*. Then, in the return motion, the end-effector of the robot moves from *B* to *A*. The optimal trajectories of the robot for the forward and return motions are plotted in Fig. 3. In this figure, the red curves show the trajectory of the end-effector. As seen in Fig. 3, the trajectory of the end-effector in the forward motion is in accordance with the trajectory of the end-effector in the return motion. The angular positions and velocities of the joints of the robot for the forward and return motions are illustrated in Figs. 4 and 5, respectively.

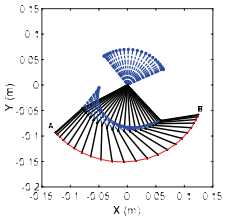

Fig. 3. The optimal trajectory of the robot.

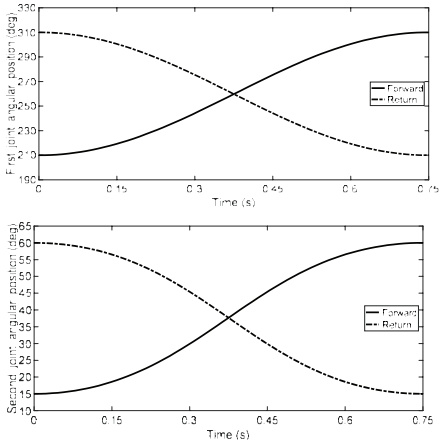

Fig. 4. Angular position of the joints.

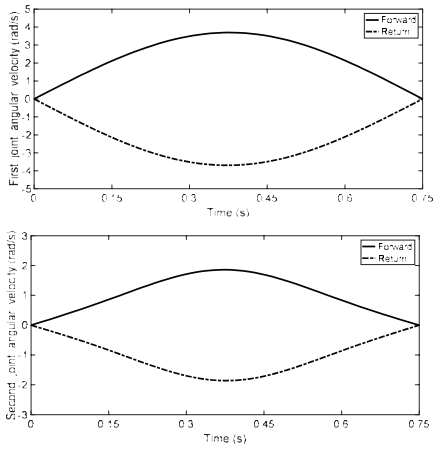

Fig. 5. Angular velocity of the joints.

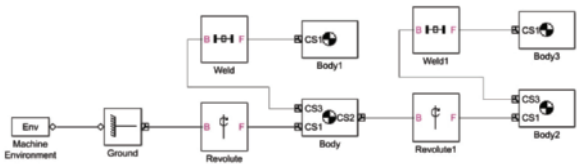

Fig. 6. Simulation of the TLRM via the Simmechanics toolbox.

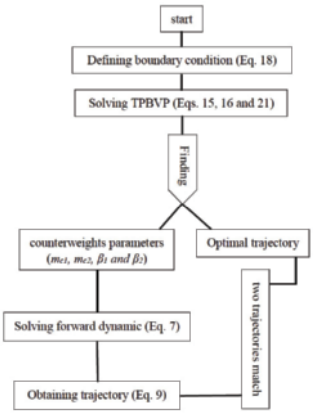

Fig. 7. The command diagram of the theoretical model.

As seen in Fig. 4, in the forward motion, the first joint moves from 210° to 310° while the second joint moves from 15° to 60°. Then, in the return motion, the first joint returns from 310° to 210°, and the second joint goes back from 60° to 15°. The time interval for both the forward and return motions is 0.75 s, making up a full-cycle period of 1.5 s.

As seen in Fig. 5, in both forward and return motions, zero angular velocity is expected at both start and end points.

The values of performance index for the forward and return motions were evaluated as 0 $(N.m)^2.s$ and 0 $(N.m)^2.s$, respectively. Thus, the torques applied at the joints 1 and 2 were found to be zero for both forward and return motions; i.e., the robot could move and return from/to the start point to/from the end point at no effort. Interestingly, the same values of parameters were obtained for the forward and return motions: m_{c1} = 381.7096 g, m_{c2} = 123.9781 g, β_1 = 175.8087° and β_2 = 189.5429°. From these results, it can be concluded that, by setting the unknown variables of the counterweights appropriately, the robot exhibited a free oscillatory motion.

In order to verify the results, the obtained parameters of counterweights and the initial conditions given in Eq. (24) were applied to the Simmechanics model of the TLRM (Fig. 6), and the forward dynamic was solved without considering any actuator, i.e. open-loop case. Flowchart of the command diagram of the model is shown in Fig. 7. Angular positions and velocities of the robot were obtained by the Simmechanics toolbox and shown in Figs. 8 and 9, respectively. These figures are plotted for three motion cycles with a period of 1.5 s.

As seen in Figs. 8 and 9, the robot exhibited a free periodic motion at a period of 1.5 s between start position *A* and end position *B*. In addition, for the time interval of 0-0.75 s, the results of the Simmechanics model are well in accordance with the results of the TPBVP (Figs. 4 and 5).

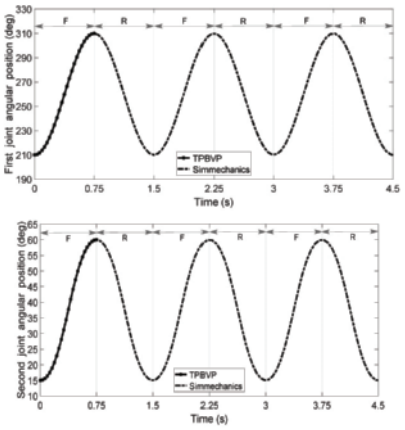

Fig. 8. Angular positions of the joints.

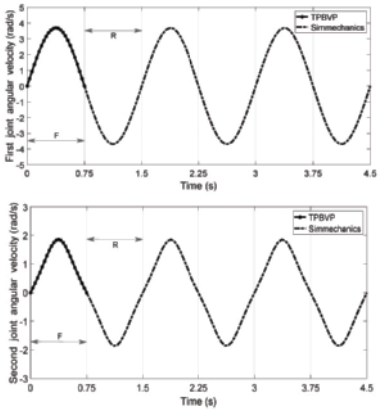

Fig. 9. Angular velocities of the joints.

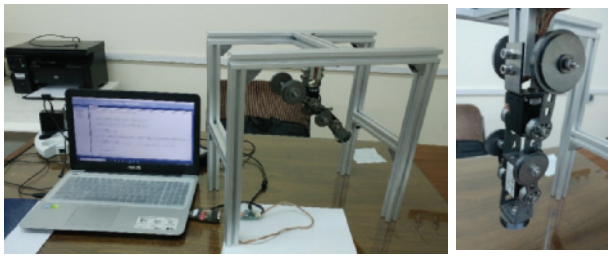

Fig. 10. The TLRM with two adjustable counterweights.

3.2 Experimental simulation

3.2.1 Experimental set-up

A TLRM with adjustable counterweights manufactured in Semnan Robotics Lab was used for the experimental implementation. The robot construction with associated counterweights are demonstrated in Fig. 10. A graded plate was used to adjust the counterweight arm angle (Fig. 11). Components of the counterweight are presented in Fig. 12. The servo-

Fig. 11. The graded circular plate.

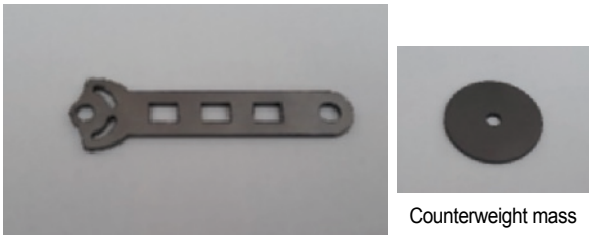

Fig. 12. Different components of the counterweight.

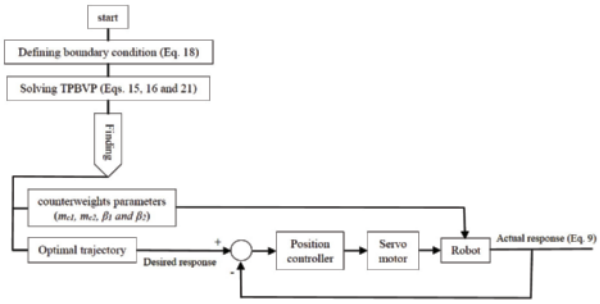

Fig. 13. Command diagram of the experimental set-up.

actuators used in the robot were Dynamixle XH430-W210 by Robotis©. Indeed, due to friction, air resistance, and parametric uncertainties, it was practically difficult to implement the motion repeatedly without consuming any power as an open-loop policy to exactly reproduce the situation in the previous section. Thus, in order to implement the proposed method, the servo-actuators were operated in position-control mode and the experimental apparatus was set up following a closed-loop approach. Flowchart of the command diagram is shown in Fig. 13.

3.2.2 Experimental results

In this experiment, the ZPB method was implemented for different pairs of start and end points. Two configurations were considered (Eq. (26)) with different positions of the coordinate system *XOY*. For two cases, the angular velocities were assumed to remain at zero at the start and end points ($\dot{\theta}_0 = \dot{\theta}_f = 0$).

$$\begin{aligned} case\,1: \quad & x_1(0) = 210\,^\circ,\ x_1(t_f) = 310\,^\circ, \\ & x_2(0) = 15\,^\circ,\ x_2(t_f) = 60\,^\circ;\ t_f = 0.75s \\ case\,2: \quad & x_1(0) = 400\,^\circ,\ x_1(t_f) = 250\,^\circ, \\ & x_2(0) = -45\,^\circ,\ x_2(t_f) = -100\,^\circ;\ t_f = 1s \end{aligned} \tag{26}$$

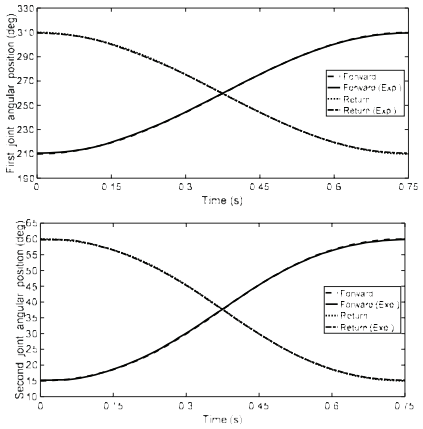

Fig. 14. Angular positions of the joints for case 1 (Exp.: Experimental).

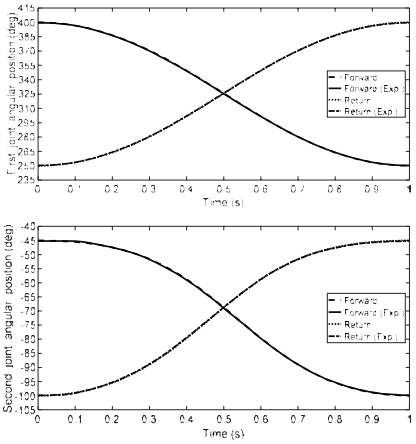

Fig. 15. Angular positions of the joints for case 2.

By solving the TPBVP, angular position and velocity at the joints and also the values of m_{c1}, m_{c2}, β_1 and β_2 of the counterweights were evaluated. Angular positions of the joints of the TLRM for the forward and return motions are illustrated in Figs. 14 and 15 for both numerical and experimental simulations.

As seen in Figs. 14 and 15, results of the TPBVP were in agreement with the results of the experimental set-up.

The angular velocities of the joints for the forward and return motions are illustrated in Figs. 16 and 17 for both simulation and experimental studies.

As seen in these figures, the results of the TPBVP were in agreement with the results of the experimental set-up.

Optimal values of the parameters m_{c1}, m_{c2}, β_1 and β_2 of counterweights for two cases are given in Table 3. For each case, the same values of parameters m_{c1}, m_{c2}, β_1 and β_2 were obtained for the forward and return motions.

For these cases, the start and finish positions of the TLRM with the counterweights are shown in Figs. 18 and 19. For the forward motion, the end-effector of the robot moves from *A* to *B*. Then, in the return motion, the end-effector of the robot moves from *B* to *A*. For case 2, the optimal trajectories of the robot for

Table 3. Optimal values of m_{c1}, m_{c2}, β_1 and β_2 for two cases.

Case	m_{c1} (g)	m_{c2} (g)	β_1 (deg)	β_2 (deg)
1	381.7096	123.9781	175.8087	189.5429
4	495.9998	133.9166	190.5673	174.2849

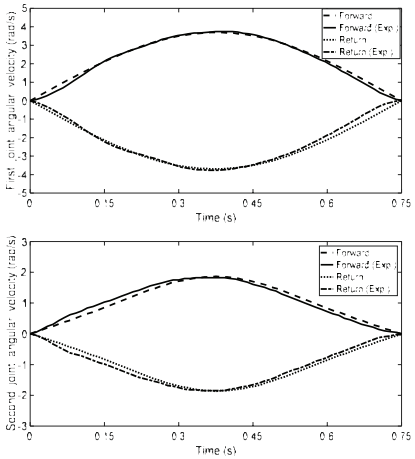

Fig. 16. Angular velocities of the joints for case 1.

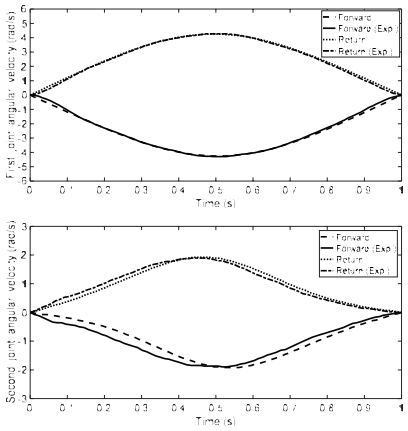

Fig. 17. Angular velocities of the joints for case 2.

the forward and return motions are plotted in Fig. 20. In this figure, the red curves show the trajectory of the end-effector. As seen in Fig. 20, the trajectory of the end-effector in the forward motion is coincides the trajectory of the end-effector in the return motion.

Numerically simulated and experimentally observed values of torque at joints of the TLRM are plotted in Figs. 21 and 22 for forward and return motions. Table 4 provides the values of the performance index under different sets of condition, as per Eq. (12).

As seen in Figs. 21 and 22, for the ZPB method, zero theoretical torque values were obtained for the forward and return motions. Also, when experimentally investigating the torque at joints upon implementing the proposed ZPB method, the obtained values were considerably lower than those under unbalanced conditions.

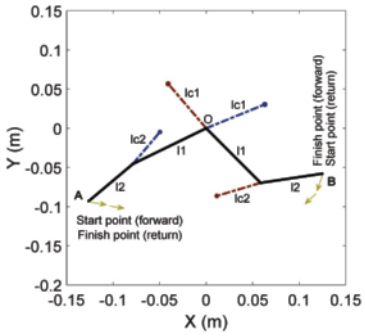

Fig. 18. The start and end points of the robot in case 1.

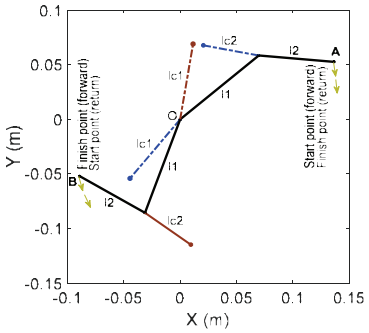

Fig. 19. The start and end points of the robot in case 2.

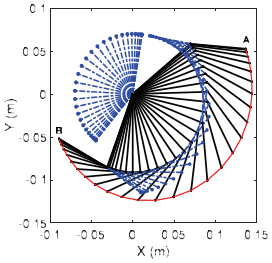

Fig. 20. The optimal trajectory of the robot in case 2.

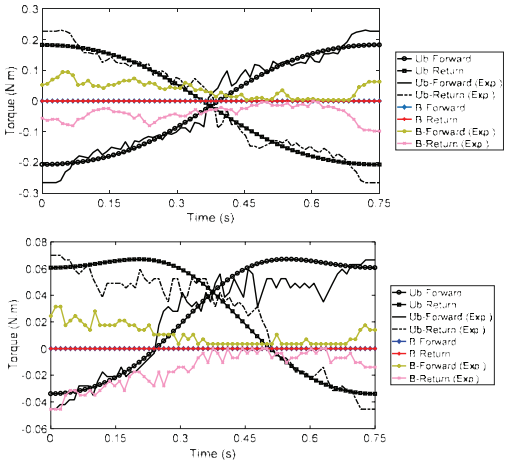

Fig. 21. Applied torque to the first (up) and second (down) joints of the robot – case 1 (Ub: Unbalanced, B: Balanced (ZPB method), Exp.: Experimental).

Table 4. The value of performance index.

Case	Condition		J ((N.m)^2.s)		
			Forward	Return	Average
1	Unbalanced	Theoretical	0.0173	0.0173	0.0173
		Experimental	0.0190	0.0191	0.0190
	Static balancing	Theoretical	0.0057	0.0057	0.0057
	Balanced (ZPB)	Theoretical	0	0	0
		Experimental	0.0016	0.0019	0.0018
2	Unbalanced	Theoretical	0.0405	0.0405	0.0405
		Experimental	0.0447	0.0451	0.0449
	Static balancing	Theoretical	0.0054	0.0054	0.0054
	Balanced (ZPB)	Theoretical	0	0	0
		Experimental	0.0027	0.0034	0.0031

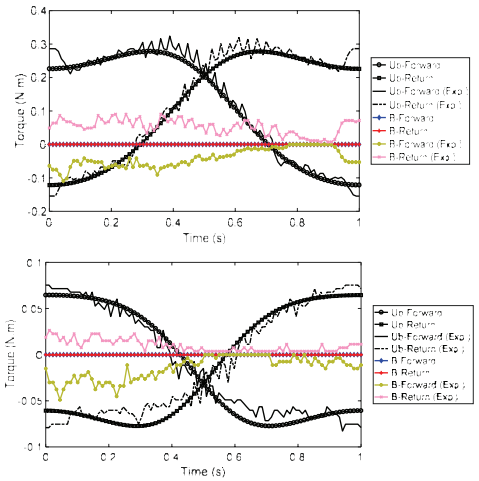

Fig. 22. Applied torque to the first (up) and second (down) joints of the robot – case 2.

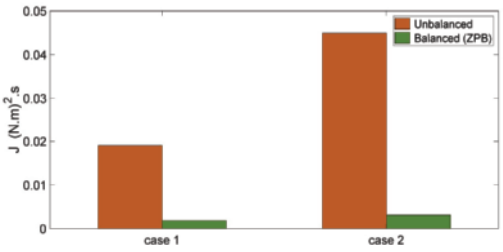

Fig. 23. The values of performance index for the experimental set-up.

As can be seen from figures, there is a difference between theoretical and experimental results. These differences are due to the friction and parameter uncertainties. Parameter uncertainties caused by measurement error of mass, length, moment of inertia and the position of the center of mass. Indeed, the used parameters in the simulation study are not identical to the actual values of the experimental model.

Based on the results presented in Table 4, the following conclusions can be drawn:

(1) Under theoretical unbalanced condition, the values of performance index for cases 1 and 2 were found to be 0.0173 and 0.0405, respectively. Under static balancing, the values of performance index for cases 1 and 2 are 0.0057 and 0.0054, respectively, while the corresponding values under theoretical ZPB were all zeros.

The static balancing reduces the performance index for cases 1 and 2, respectively, 67.05 %, and 86.67 %, while the ZPB method reduces the performance index for two cases 100 %. Note that the performance index in the static balancing is increased for high-speed task.

(2) Under experimental unbalanced condition, the values of performance index for cases 1 and 2 were found to be 0.0190 and 0.0449, respectively, while the corresponding values under experimental balanced condition were 0.0018 and 0.0031, respectively. Therefore, the ZPB method reduces the performance index for cases 1 and 2, respectively, 90.53 %, and 93.10 %.

Plotted in Fig. 23 are the values of the performance index under experimental condition for two cases. This figure demonstrates the efficiency of ZPB method in comparison with the unbalanced condition.

4. Conclusions

In this paper, zero-power balancing (ZPB) method was presented for a two-link robotic manipulator (TLRM) using an indirect solution of the optimal control problem. In the proposed methodology, the states, joint torques, and unknown parameters of counterweights were determined simultaneously, ending up with zero performance index. Therefore, by achieving the performance index to the optimal value, the values of states and counterweights parameters are optimum for the predefined point-to-point task. The necessary conditions for optimality of the TLRM were derived using the PMP. Indeed, for a point-to-point motion, the values of m_{c1}, m_{c2}, β_1 and β_2 of the counterweights were obtained in such a way to have the TLRM oscillated freely between the start and end points. By applying the optimal values of m_{c1}, m_{c2}, β_1 and β_2 of the counterweights to the Simmechanics model of the TLRM, the robot was proved to be able to oscillate between initial and final angles at no power consumption. In order to demonstrate efficiency of the proposed method, it was applied experimentally. In the practical implementation, significantly lower performance index values were obtained with the robot on which the proposed methodology was applied, as compared to the unbalanced robot.

References

[1] E. I. Rivin, *Mechanical Design of Robots*, New York, McGraw-Hill (1988).

[2] R. Saravanan, S. Ramabalan and P. D. Babu, Optimum static balancing of an industrial robot mechanism, *Engineering Appli-*

cations of Artificial Intelligence, 21 (6) (2008) 824-834.
[3] T. A. H. Coelho, L. Yong and V. F. A. Alves, Decoupling of dynamic equations by means of adaptive balancing of 2-dof open-loop mechanisms, *Mechanism and Machine Theory,* 39 (8) (2004) 871-881.
[4] C. M. Gosselin, F. Vollmer, G. Cote and Y. Wu, Synthesis and design of reactionless three-degree-of-freedom parallel mechanisms, *IEEE Transactions on Robotics and Automation,* 20 (2) (2004) 191-199.
[5] M. Moradi, A. Nikoobin, and S. Azadi, Adaptive decoupling for open chain planar robots, *Scientia Iranica. Transaction B, Mechanical Engineering*, 17 (5) (2010) 376.
[6] C. Cho and S. Kang, Design of a static balancing mechanism for a serial manipulator with an unconstrained joint space using one-DOF gravity compensators, *IEEE Transactions on Robotics,* 30 (2) (2013) 421-431.
[7] K. Chaudhary and H. Chaudhary, Dynamic balancing of planar mechanisms using genetic algorithm, *Journal of Mechanical Science and Technology,* 28 (10) (2014) 4213-4220.
[8] S. Veer and S. Sujatha, Approximate spring balancing of linkages to reduce actuator requirements, *Mechanism and Machine Theory,* 86 (2015) 108-124.
[9] L. Chen, Z. Yan and Z. Du, Optimal design of dynamic balancing for the redundant orientation mechanism of a master manipulator, *International Conference on Mechatronics and Automation (ICMA),* IEEE (2015).
[10] J. Boisclair, P. L. Richard, T. Laliberte and C. Gosselin, Gravity compensation of robotic manipulators using cylindrical halbach arrays, *IEEE/ASME Transactions on Mechatronics,* 22 (1) (2016) 457-464.
[11] D. S. Kumani and H. Chaudhary, Minimizing constraint forces and moments of manipulators using teaching-learning-based optimization and octahedron point mass model, *Proceedings of the Institution of Mechanical Engineers, Part C: Journal of Mechanical Engineering Science,* 232 (19) (2018) 3500-3511.
[12] Y. Zhang, V. Arakelian and J. P. L. Baron, Linkage design for gravity balancing by means of non-zero length springs, *ROMANSY 22–Robot Design, Dynamics and Control,* Springer, Cham. (2019) 163-170.
[13] X. Yun, X. Mei, G. Jiang and B. Wang, A new dynamic balancing method of spindle based on the identification energy transfer coefficient, *Journal of Mechanical Science and Technology,* 33 (10) (2019) 4595-4604.
[14] A. Martini, M. Troncossi and A. Rivola, Algorithm for the static balancing of serial and parallel mechanisms combining counterweights and springs: Generation, assessment and ranking of effective design variants, *Mechanism and Machine Theory,* 137 (2019) 336-354.
[15] T. Ravichandran, D. Wang and G. Heppler, Simultaneous plant-controller design optimization of a two-link planar manipulator, *Mechatronics,* 16 (3-4) (2006) 233-242.
[16] A. Nikoobin and M. Moradi, Optimal balancing of the robotic manipulators, *Dynamic Balancing of Mechanisms and Synthesizing of Parallel Robots,* Springer, Cham. (2016) 337-363.
[17] A. Nikoobin and M. Moradi, Optimal balancing of robot manipulators in point-to-point motion, *Robotica,* 29 (2) (2011) 233-244.
[18] A. Nikoobin, M. Moradi and A. Esmaili, Optimal spring balancing of robot manipulators in point-to-point motion, *Robotica,* 31 (4) (2013) 611-621.
[19] A. Nikoobin, M. R. Vezvari and M. Ahmadieh, Optimal balancing of planar cable robot in point to point motion using the indirect approach, *2015 3rd RSI International Conference on Robotics and Mechatronics (ICROM),* IEEE (2015).
[20] M. R. Vezvari and A. Nikoobin, Optimal balancing of spatial suspended cable robot in point-to-point motion using indirect approach, *International Journal of Advanced Design & Manufacturing Technology,* 10 (3) (2017) 89-98.
[21] M. Moradi, M. Naraghi and E. A. Kamali, Simultaneous design of parameters and controller of robotic manipulators: Closed loop approach to practical implementation, *Advanced Robotics,* 32 (3) (2018) 105-121.
[22] T. Chettibi, H. E. Lehtihet, M. Haddad and S. Hanchi, Minimum cost trajectory planning for industrial robots, *European Journal of Mechanics-A/Solids,* 23 (4) (2004) 703-715.
[23] H. R. Heidari, M. H. Korayem, M. Haghpanahi and V. F. Batlle, Optimal trajectory planning for flexible link manipulators with large deflection using a new displacements approach, *Journal of Intelligent & Robotic Systems,* 72 (3-4) (2013) 287-300.
[24] M. H. Korayem and M. Irani, New optimization method to solve motion planning of dynamic systems: Application on mechanical manipulators, *Multibody System Dynamics,* 31 (2) (2014) 169-189.
[25] M. H. Ghasemi, N. Kashiri and M. Dardel, Time-optimal trajectory planning of robot manipulators in point-to-point motion using an indirect method, *Proceedings of the Institution of Mechanical Engineers, Part C: Journal of Mechanical Engineering Science,* 226 (2) (2012) 473-484.
[26] S. Gong, R. Alqasemi and R. Dubey, Gradient optimization of inverse dynamics for robotic manipulator motion planning using combined optimal control, *ASME 2017 International Mechanical Engineering Congress and Exposition* (2017).
[27] D. E. Kirk, *Optimal Control Theory: An Introduction*, Prentice-Hall, Englewood Cliffs, New Jersey (1970).

Mojtaba Riyahi Vezvari is a Ph.D. student of Mechanical Engineering in University of Semnan, Iran. He received his B.Sc. in Mechanical Engineering at Semnan University, Iran, in 2012 and his M.Sc. in Mechanical Engineering at the same university, in 2014. His research interests are robotic, optimization, dynamic and control.

Amin Nikoobin is an Assistant Professor of Mechanical engineering at the University of Semnan, Iran. He received his B.Sc. in Mechanical Engineering at Isfahan University of Technology, Iran, in 2001. He received his M.Sc. in Mechanical Engineering at Iran University of Science and Technology, in 2003 and his Ph.D. in Mechanical Engineering at the same university in 2007. His research interests are robotic, control and dynamic.

Ali Ghoddosian is an Associate Professor of Mechanical Engineering at the University of Semnan. He received his B.S. in Mechanical Engineering from Shahid Chamran University, Iran in 1989 and his M.S. in Mechanical Engineering from Iran University of Science and Technology in 1993. He received his Ph.D. in Mechanical Engineering from I.I.T Delhi University, India in 2000. His research interests are finite element, structural optimization and numerical optimization.